Residual CO_2 imaged with X-ray micro-tomography

Stefan Iglauer,[1] Adriana Paluszny,[2] Christopher H. Pentland,[2] and Martin J. Blunt[2]

Received 15 September 2011; revised 7 October 2011; accepted 11 October 2011; published 10 November 2011.

[1] Carbon capture and storage (CCS), where CO_2 is injected into geological formations, has been identified as an important way to reduce CO_2 emissions to the atmosphere. While there are several aquifers worldwide into which CO_2 has been injected, there is still uncertainty in terms of the long-term fate of the CO_2. Simulation studies have proposed capillary trapping – where the CO_2 is stranded as pore-space droplets surrounded by water – as a rapid way to secure safe storage. However, there has been no direct evidence of pore-scale trapping. We imaged trapped super-critical CO_2 clusters in a sandstone at elevated temperatures and pressures, representative of storage conditions using computed micro-tomography (μ-CT) and measured the distribution of trapped cluster size. The clusters occupy 25% of the pore space. This work suggests that locally capillary trapping is an effective, safe storage mechanism in quartz-rich sandstones. **Citation:** Iglauer, S., A. Paluszny, C. H. Pentland, and M. J. Blunt (2011), Residual CO_2 imaged with X-ray micro-tomography, *Geophys. Res. Lett.*, *38*, L21403, doi:10.1029/2011GL049680.

1. Introduction

[2] With increasing fossil-fuel consumption accounting for more than 80% of energy use [*International Energy Agency*, 2010], CCS is seen as a key technology to tackle greenhouse gas emissions directly at source [*Intergovernmental Panel on Climate Change* (*IPCC*) 2005]. Once captured and transported, the CO_2 is injected at depths of 800m or more where the CO_2 is in a dense supercritical (sc) state. Deep saline aquifers are likely to have the highest storage capacities because of their geographical abundance and large available volumes [*IPCC*, 2005]. The principal concern with CCS is to ensure that the CO_2 remains underground. There are four trapping mechanisms that prevent the CO_2 from escaping: a) stratigraphic, where a layer of caprock blocks the buoyant CO_2 from flowing upwards [*Hesse et al.*, 2008]; b) dissolution into the formation brine, where the dense CO_2-saturated brine sinks through the aquifer [*Riaz et al.*, 2006]; c) mineral trapping where dissolved CO_2 reacts with formation brine or host rock to form solid minerals [*Xu et al.*, 2003] and d) capillary trapping [*Hesse et al.*, 2008; *Juanes et al.*, 2006; *Qi et al.*, 2009]. In the fourth process, capillary trapping, the focus of this work, it is hypothesized that the CO_2 is immobilized by capillary forces as pore-space bubbles. When the injected CO_2 plume rises upwards it is followed by groundwater influx; at the trailing edge of the CO_2 plume the CO_2 is displaced by water and a fraction of the CO_2 is trapped. This process, analogous to the trapping of oil during waterflooding in hydrocarbon reservoirs, has been proposed as the most rapid and effective way to ensure safe storage that can be engineered through brine injection [*Qi et al.*, 2009].

2. Experimental Procedure

[3] We imaged trapped clusters of $scCO_2$ directly in a homogeneous sandstone (Doddington) with a porosity of 20.7% and a brine permeability of 1.58×10^{-12} m^2. Doddington consists of 98 wt% α-quartz, 2 wt% K-feldspar and traces of kaolinite (measured by X-ray diffraction on a Philips PW1830 diffractometer). A cylindrical core (9 mm length and 4.95 mm diameter) was drilled and placed in a specially developed μ-CT cell capable of operating at high pressure and elevated temperature (HPET). The novel HPET μ-CT cell is an assembly of an inner pressure module (core assembly) which housed the sandstone, and an outer carbon fiber vessel which contained confining fluid (Figure 1). Two stainless steel flow heads sealed the carbon fiber vessel so that pressure could be maintained constant. The core was wrapped in thin aluminium foil (50 μm thick) to prevent $scCO_2$ from escaping. $scCO_2$ is an excellent solvent and would otherwise penetrate into the fluoropolymer elastomer (Viton) sleeve, which was placed around the foil. The sleeve was compressed by the confining fluid so that fluid bypassing around the core was prevented. This is essentially a miniaturized Hassler cell [*Hassler*, 1944] design. The apparatus guaranteed that confining fluid and pore fluids were hydraulically separated. Fluid injection occurred through the steel flow heads and into the sealed core through stainless steel tubing. The core assembly had an inlet and outlet for fluid injection and production.

[4] The core was initially fully saturated with brine, then CO_2 was injected (primary drainage), representing the initial migration of CO_2 through the aquifer. This was followed by a waterflooding step, where brine saturated with CO_2 was injected. This represents the trailing edge of an advancing CO_2 plume, or when brine is artificially injected: some CO_2 is displaced, leaving behind an immobile residual fraction. Experimental flow, pressure and temperature conditions in the core were representative of a deep saline aquifer at approximately 1000 m depth (T = 323 K [= 50°C], 9 MPa pore pressure and 11.75 MPa overburden pressure).

[5] Specifically, the μ-CT experiment consisted of following steps (Figure 1a):

[6] 1. The core was vacuumed and then fully saturated with brine (10wt% potassium iodide, KI, was dissolved in deionized water to enhance the CT contrast; NaCl brine would have resulted in low CT contrast between brine and CO_2).

[7] 2. The space between core assembly and carbon fiber vessel was filled with deionized water, which acted as a confining fluid. This confining space was connected through

[1]Department of Petroleum Engineering, Curtin University, Perth, Western Australia, Australia.
[2]Department of Earth Science and Engineering, Imperial College London, London, UK.

Copyright 2011 by the American Geophysical Union.
0094-8276/11/2011GL049680

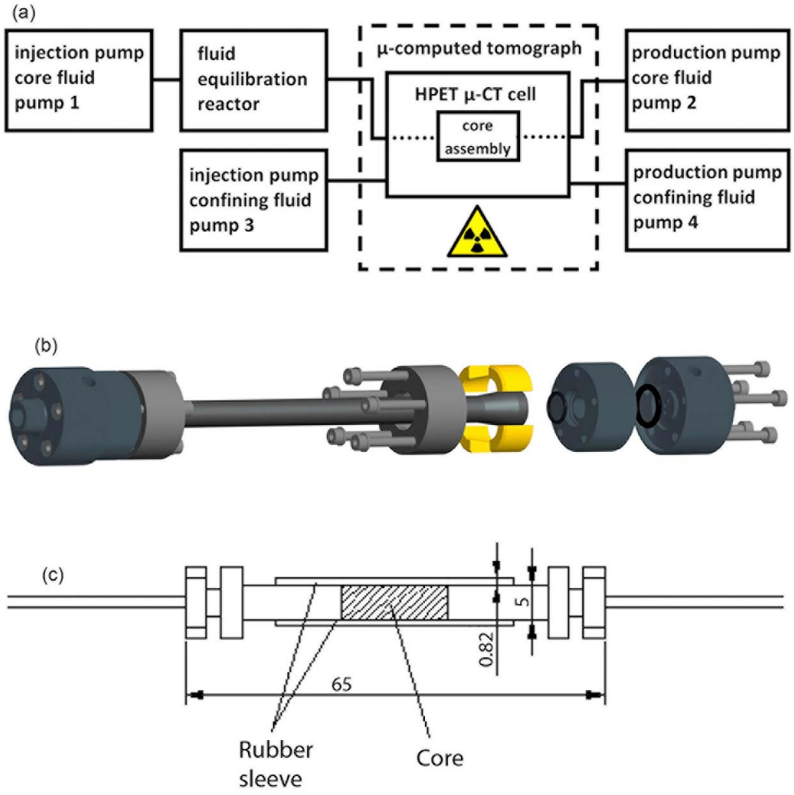

Figure 1. Sketch of the experimental setup: (a) process scheme; (b) assembly plot of the high pressure elevated temperature (HPET) μ-CT cell; (c) core assembly (the thin aluminium foil is not shown), dimensions in millimeters. The core assembly is housed in a thin-walled (1mm wall thickness) carbon fiber vessel.

the steel heads with thermally isolated steel tubing to two syringe pumps. One pump pumped confining fluid into the confining space and the second pump received confining fluid while maintaining constant high pressure conditions (11.75 MPa). The confining fluid was continuously heated in both pumps so that isothermal conditions in the core were achieved (323 K). In addition a heating jacket was placed around the top end of the carbon fiber vessel to support isothermal conditions.

[8] 3. Two syringe pumps which were connected with thermally isolated steel tubing to the core assembly's inlet and outlet then increased the pore pressure to 9 MPa.

[9] 4. Once the viscoelastic rubber sleeve relaxed to the pressure and the core and the pore fluids were heated to 323 K, the 10wt% KI brine was displaced with 10wt% KI brine which was saturated with $scCO_2$ at the same thermophysical conditions (323 K, 9 MPa) in a separate mixing reactor.

[10] 5. After pumping at least 1000 pore volumes (PV) of CO_2-saturated brine through the core, $scCO_2$ was injected in a primary drainage process, again at constant thermophysical conditions. Approximately 1000 PV of $scCO_2$ were injected at a flow rate of 2 mL/min (which corresponds to a capillary number N_{cap} of 10^{-6}; $N_{cap} = \frac{\nu\mu}{\sigma}$ with the Darcy velocity ν, the $scCO_2$ viscosity μ (= 2.1×10^{-5} Pa.s) [*Fenghour et al.*, 1998] and the $scCO_2$-brine interfacial tension σ (= 36.0 mN/m) [*Chalbaud et al.*, 2009]).

[11] 6. The core was scanned with a GE phoenix | X-ray microtomography system v/tome/x to obtain an image for the initial $scCO_2$ saturation and distribution in the core at a nominal resolution of 13.156 μm. This experiment (starting with step 1) was repeated three times to check reproducibility. Similar results were obtained for each scan and reproducibility was good.

[12] 7. In the waterflooding step approximately 50 PV of CO_2-saturated brine were injected at isothermal and isobaric conditions and at a flow rate of 2 mL/min which corresponded to a capillary number of 2.45×10^{-5} (CO_2 saturated brine viscosity = 5.1×10^{-4} Pa.s) [*Bando et al.*, 2003]. The brine was CO_2 saturated so as not to dissolve the $scCO_2$ phase. Changes in $scCO_2$ saturation were only due to immiscible displacements within the pore space.

[13] 8. The sample was scanned with the μ-CT instrument at a nominal resolution of 13.682 μm. Three complete independent experiments were repeated to check reproducibility; tomographic images were similar for each replicate and gave the same average residual saturations and cluster size distributions.

[14] During each scan, at the end of primary drainage and waterflooding, 720 radiographs were obtained and reconstructed. The raw μ-CT images were cleaned of ring artefacts by applying a stripe removal algorithm based on combined wavelet—Fourier filtering [*Münch et al.*, 2009]. No median filter was applied during this process. Salt-and-pepper noise was removed using an anisotropic regularization filter [*Tschumperlé and Deriche*, 2003]. The phases were segmented according to their CT contrast using multi-thresholding, i.e., by identifying peaks in the gray-level histogram of each image based on Otsu's algorithm [*Otsu*, 1979]. Primary drainage images are shown in Figure 2.

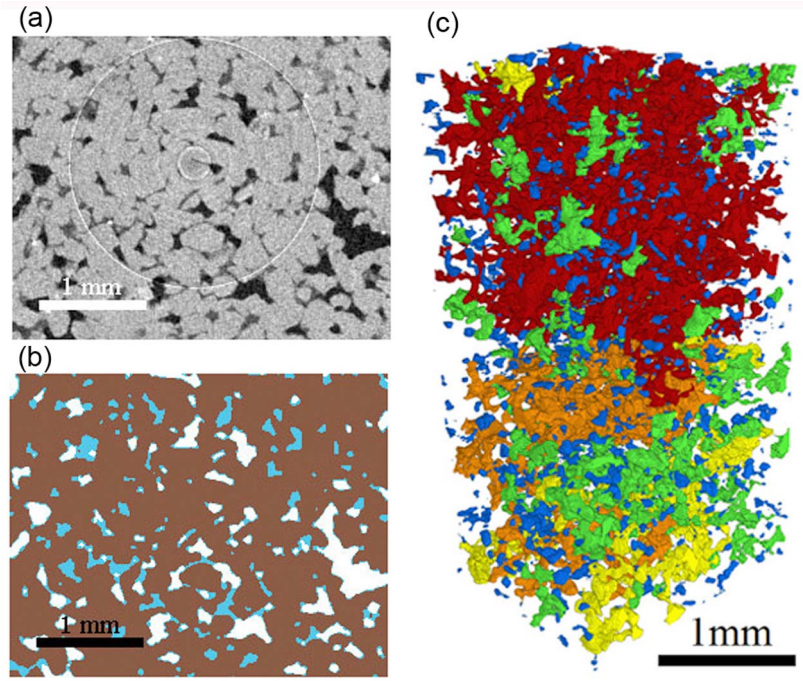

Figure 2. Images showing the core after primary drainage with $scCO_2$ (nominal voxel resolution is 13.156 μm): (a) two dimensional slice through the core; $scCO_2$ is black, brine is dark grey and sandstone is light grey. The few white areas are minerals with high X-ray absorption. The area shown is 2.828 mm × 3.525 mm ≈ 9.97 mm^2 (215 × 268 pixels); (b) same slice with phases segmented. $scCO_2$ is white, brine light blue and rock is brown; (c) $scCO_2$ clusters in three dimensions, the volume displayed is 3.525 mm × 2.828 mm × 6.578 mm ≈ 65.60 mm^3 (268 × 215 × 500 voxels), the clusters are colored according to size: blue <1000 voxels, green 1000-10000 voxels, yellow 10000-100000 voxels, orange 10^5–10^6, red >10^6 voxels.

Images taken after waterflooding are shown in Figure 3; the end sections contained significant noise and were cropped. Animations (Animations S1–S3) of Figures 2c, 3c and the largest trapped $scCO_2$ cluster are available in the auxiliary material.[1]

3. Results and Discussion

[15] We measured porosity, initial CO_2 saturations (after primary drainage) and residual CO_2 saturations (after waterflooding) on the μ-CT images; these are consistent with literature results measured with Helium pycnometry [*Iglauer et al.*, 2010] and standard core floods on larger samples [*Pentland et al.*, 2011; *Suekane et al.*, 2008] (Table 1).

[16] The amount of trapping is controlled by the competition between snap-off and piston-like advance [*Blunt and Scher*, 1995]. In a strongly water-wet medium (a wetting phase-non-wetting phase contact angle close to zero), water flows along the roughness in wetting layers and during waterflooding these layers swell, filling the narrowest regions of the pore space in order of size by snap-off [*Roof*, 1970]. This is a percolation-like process that leads to trapping of the non-wetting phase in the larger pores. Percolation theory predicts that there is a power-law distribution of the number of trapped clusters of size s: $N \sim s^{-\tau}$ with an exponent τ = 2.189 [*Lorenz and Ziff*, 1998]. As the contact angle increases, snap-off is less favoured and the dominant mode of displacement is cooperative piston-like advance, where a water front moves through the system; when snap-off is completely suppressed there is little or no trapping [*Blunt and Scher*, 1995]. As discussed below $scCO_2$/brine/sandstone is not strongly water-wet; this results in less capillary trapping (less snap-off) and a nominally reduced power law coefficient τ, with fewer small residual CO_2 clusters.

[17] Figures 2 and 3 illustrate that $scCO_2$ is the non-wetting phase under these conditions; brine contacts the rock surface and fills the smaller pores; CO_2 preferentially resides in the centers of the larger pore spaces and is trapped in clusters of different size, surrounded by brine. During primary drainage, the CO_2 is connected in large clusters; some snap-off to maintain local capillary equilibrium is observed that breaks up the injected phase [*Roof*, 1970; *Lenormand et al.*, 1988]. The residual $scCO_2$ saturation, composed of clusters of all sizes, is consistent with values measured in larger scale core floods [*Pentland et al.*, 2011; *Suekane et al.*, 2008]. However, the residual CO_2 saturation (24.9%) measured is lower than in the case of an analogue, strongly water-wet, Doddington sandstone-n-octane-brine experiment where a residual oil saturation of 35% was observed [*Iglauer et al.*, 2010] (Table 1). Based on the discussion above, this implies an increased water contact angle on the quartz surface at high pressures, as observed on smooth surfaces [*Chiquet et al.*, 2007] and in relative permeability experiments [*Berg et al.*, 2011].

[18] We explored the implication of a lower overall residual saturation on the distribution of trapped clusters by

[1]Auxiliary materials are available in the HTML. doi:10.1029/2011GL049680.

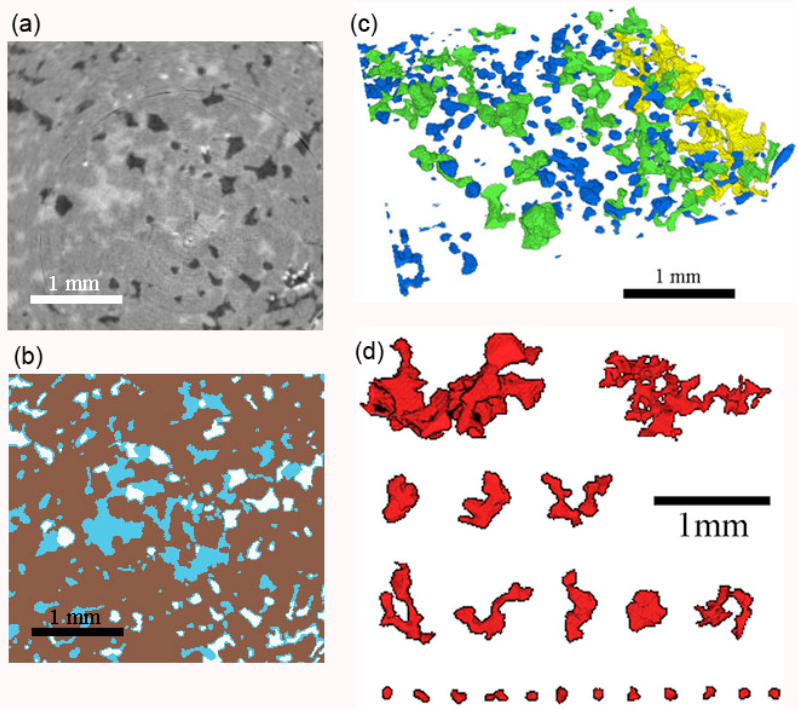

Figure 3. Images showing the core after waterflooding with CO_2 saturated brine (secondary imbibition) (nominal voxel resolution is 13.682 μm): (a) two dimensional slice through the core; $scCO_2$ is black, brine is light grey and sandstone is dark grey. The few white areas are minerals with high X-ray absorption. The area shown is 3.434 mm × 3.144 mm ≈ 10.80 mm^2 (261 × 239 pixels); (b) same slice with phases segmented. $scCO_2$ is white, brine light blue and rock is brown; (c) trapped $scCO_2$ clusters in three dimensions, the volume displayed is 3.433 mm × 3.144 mm × 0.658 mm ≈ 7.10 mm^3 (261 × 239 × 50 voxels), the clusters are colored according to size: blue <1000 voxels, green 1000–5700 voxels, yellow >5700 voxels; (d) selected trapped clusters of different sizes, top row: the two largest clusters (19496 and 16165 voxels), second row: 4500–5700 voxels, third row: 3000–4000 voxels (medium sized clusters), bottom row: 150–200 voxels (small clusters).

counting the number of disconnected $scCO_2$ clusters $N(s)$ of size s in voxels. We define the cumulative cluster size distribution [*Dias and Wilkinson*, 1986] $S(s) = \sum_{s}^{\infty} sn(s) \propto s^{-\tau+2}$ where $n(s) = N(s)/N_v$ and N_v is the total number of pore-space voxels. $S(s)$ represents the contribution to the trapped CO_2 saturation of clusters larger than a size s; $S(1)$ is the residual saturation. Figure 4 shows $n(s)$ and $S(s)$ compared to results obtained in the same rock for trapped oil (n-octane) at ambient conditions [*Iglauer et al.*, 2010]. Other authors have imaged residual saturation and measured the cluster-size distribution for ambient-condition experiments [*Kumar et al.*, 2010; *Prodanović et al.*, 2007; *Karpyn et al.*, 2010]. In a strongly water-wet system (oil-brine), we find an approximately power-law size distribution with $\tau = 2.05$, close to the prediction from percolation theory [*Blunt and Scher*, 1995]; $S(s)$ only drops sharply when the clusters begin to span the system, which represents the largest sizes we can see in the experiment. With $scCO_2$ (Figure 4) we see a lower residual saturation and fewer small residual clusters; the best fit to the data gives $\tau = 2.01$. We see fewer clusters occupying one or a small number of pores ($s \sim 30$), with a larger contribution from bigger clusters (spanning 10 or more pores; $s > 300$) than in the strongly water-wet system. It would appear that locally snap-off is suppressed, but there are still – at larger scales – many isolated clusters, implying that filling of some of the very narrowest pore spaces with brine during imbibition is sufficient to trap a significant fraction of the non-wetting CO_2 phase. At the capillary numbers studied, capillary forces still dominate the displacement over the length of the volume imaged [*Hilfer and Øren*, 1996] and so we do not expect the results to be affected by viscous mobilization of the largest clusters.

Table 1. Porosities and CO_2 Saturations

	Porosity μ-CT [%]	Porosity He[a] [%]	CO_2 Saturation μ-CT [%]	CO_2 Saturation Coreflood[b] [%]	Oil Saturation μ-CT [%][c]	Oil Saturation Coreflood[b] [%]
Primary drainage	20.5	20.7	48.0 (initial)	50 (initial)	not measured (initial)	44(initial)
Waterflooding	20.8	20.7	24.9 (residual)	25 (residual)	35.0 (residual)	35 (residual)

[a]Measured via Helium pycnometry on a larger core sample of the same rock [*Iglauer et al.*, 2010].
[b]Measured with the porous plate method on a Berea sandstone core (porosity = 0.22 and brine permeability = 4.6×10^{-13} m^2) [*Pentland et al.*, 2011].
[c]Measured in a similar μ-CT experiment with the same rock with n-octane at ambient conditions [*Iglauer et al.*, 2010].

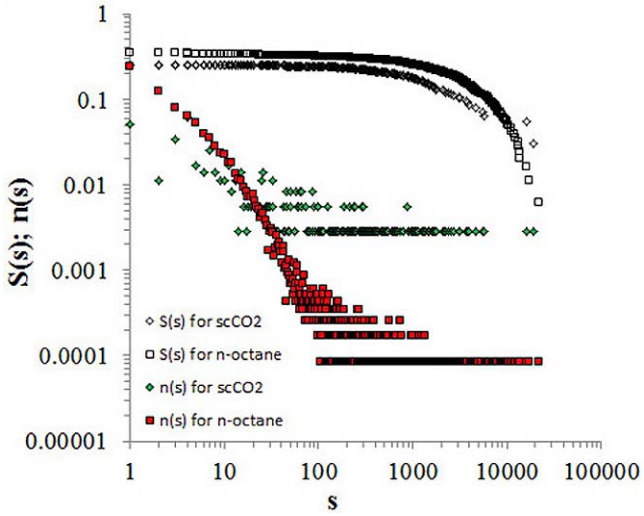

Figure 4. The normalized cluster size distribution $n(s)$ and $S(s)$, the fractional pore volume occupied by clusters larger than a size s, as a function of cluster size on doubly logarithmic axes. $S(s)$ indicates the contribution to residual saturation from clusters of size s or greater. Data for $scCO_2$ are compared to analogue experiments on the same rock type performed at ambient conditions for a strongly water-wet octane-brine system [*Iglauer et al.*, 2010]. A cluster size s = 30 represents, approximately, a cluster filling a single pore.

Furthermore, the principal contribution to residual saturation comes from clusters that are significantly smaller than the system size: it is possible that poor sampling of the largest clusters could lead to an error of around 2% in the estimate of large-scale residual saturation.

[19] Future research will focus on investigating the role of rock type on capillary trapping. We show here that CO_2 can be trapped in a relatively clean quartz rich sandstone. Carbonate rocks and sandstones containing clays and other mineral impurities may show different trapping behavior due to the influence of surface chemistry on contact angle and hence snap–off.

4. Conclusions

[20] We have used a novel high-pressure elevated-temperature micro-flow cell to image trapped clusters of super-critical CO_2 at the pore scale confirming that capillary trapping of $scCO_2$ is locally a viable CCS mechanism in clean sandstones. While there is a lower residual saturation than for an analogue strongly water-wet system, with fewer small clusters, there are clusters of all sizes, up to the system size, providing a large surface area for dissolution and reaction [*Hirai et al.*, 1997] leading, again, to reduced CO_2 leakage risk.

[21] **Acknowledgments.** We would like to thank Shell under the Shell-Imperial College Grand Challenge on Clean Fossil Fuels for funding this work.

[22] The Editor thanks the two anonymous reviewers for their assistance in evaluating this paper.

References

Bando, S., F. Takemura, M. Nishio, E. Hihara, and M. Akai (2003), Solubility of CO_2 in aqueous solutions of NaCl at (30 to 60) °C and (10 to 20) MPa, *J. Chem. Eng. Data*, *48*(3), 576–579, doi:10.1021/je0255832.

Berg, S., S. Oedai, and H. Ott (2011), Displacement and mass transfer between saturated and unsaturated CO_2-brine systems in sandstone, *Int. J. Greenhouse Gas Control*, doi:10.1016/j.ijggc.2011.04.005, in press.

Blunt, M. J., and H. Scher (1995), Pore-level modeling of wetting, *Phys. Rev. E*, *52*(6), 6387–6403, doi:10.1103/PhysRevE.52.6387.

Chalbaud, C., M. Robin, J. Lombard, F. Martin, P. Egermann, and H. Bertin (2009), Interfacial tension measurements and wettability evaluation for geological CO_2 storage, *Adv. Water Resour.*, *32*, 98–109, doi:10.1016/j.advwatres.2008.10.012.

Chiquet, P., D. Broseta, and S. Thibeau (2007), Wettability alteration of caprock minerals by carbon dioxide, *Geofluids*, *7*, 112–122, doi:10.1111/j.1468-8123.2007.00168.x.

Dias, M. M., and D. Wilkinson (1986), Percolation with trapping, *J. Phys. A Math Nucl. Gen.*, *19*, 3131–3146, doi:10.1088/0305-4470/19/15/034.

Fenghour, A., W. A. Wakeham, and V. Vesovic (1998), The viscosity of carbon dioxide, *J. Phys. Chem. Ref. Data*, *27*(1), 31–44, doi:10.1063/1.556013.

Hassler, G. L. (1944), Method and apparatus for permeability measurements, Patent 2,345,935, U.S. Patent and Trademark Off., Washington, D. C.

Hesse, M. A., F. M. Orr, and H. A. Tchelepi (2008), Gravity currents with residual trapping, *J. Fluid Mech.*, *611*, 35–60, doi:10.1017/S002211200800219X.

Hilfer, R., and P. E. Øren (1996), Dimensional analysis of pore scale and field scale immiscible displacement, *Transp. Porous Media*, *22*, 53–72, doi:10.1007/BF00974311.

Hirai, S., K. Okazaki, H. Yazawa, H. Ito, Y. Tabe, and K. Hijikata (1997), Measurement of CO_2 diffusion coefficient and application of LIF in pressurized water, *Energy*, *22*(2–3), 363–367, doi:10.1016/S0360-5442(96)00135-1.

Iglauer, S., S. Favretto, G. Spinelli, G. Schena, and M. J. Blunt (2010), X-ray tomography measurements of power-law cluster size distributions for the non-wetting phase in sandstones, *Phys. Rev. E*, *82*(5), 056315, doi:10.1103/PhysRevE.82.056315.

Intergovernmental Panel on Climate Change (IPCC) (2005), *IPCC Special Report on Carbon Dioxide Capture and Storage. Prepared by Working Group III of the Intergovernmental Panel on Climate Change*, edited by B. Metz et al., Cambridge Univ. Press, Cambridge, U. K.

International Energy Agency (2010), *Key World Energy Statistics*, Paris.

Juanes, R., E. J. Spiteri, F. M. Orr, and M. J. Blunt (2006), Impact of relative permeability hysteresis on geological CO_2 storage, *Water Resour. Res.*, *42*, W12418, doi:10.1029/2005WR004806.

Karpyn, Z., M. Piri, and G. Singh (2010), Experimental investigation of trapped oil clusters in a water-wet bead pack using X-ray microtomography, *Water Resour. Res.*, *46*, W04510, doi:10.1029/2008WR007539.

Kumar, M., T. Senden, A. Sheppard, J. Middleton, and M. Knackstedt (2010), Visualizing and quantifying the residual phase distribution in core material, *Petrophysics*, *51*(5), 323–332.

Lenormand, R., E. Touboul, and C. Zarcone (1988), Numerical models and experiments on immiscible displacements in porous media, *J. Fluid Mech.*, *189*, 165–187, doi:10.1017/S0022112088000953.

Lorenz, C. D., and R. M. Ziff (1998), Precise determination of the bond percolation thresholds and finite-size scaling corrections for the sc, fcc and bcc lattices, *Phys. Rev. E*, *57*(1), 230–236, doi:10.1103/PhysRevE.57.230.

Münch, B., P. Trtik, F. Marone, and M. Stampanoni (2009), Stripe and ring artefact removal with combined wavelet—Fourier filtering, *Opt. Express*, *17*(10), 8567–8591, doi:10.1364/OE.17.008567.

Otsu, N. (1979), A threshold selection method from gray-level histograms, *IEEE Trans. Syst. Man Cybern.*, *9*(1), 62–66, doi:10.1109/TSMC.1979.4310076.

Pentland, C. H., R. El-Maghraby, S. Iglauer, and M. J. Blunt (2011), Measurements of the capillary trapping of super-critical carbon dioxide in Berea Sandstone, *Geophys. Res. Lett.*, *38*, L06401, doi:10.1029/2011GL046683.

Prodanović, M., W. B. Lindquist, and R. S. Seright (2007), 3D image-based characterization of fluid displacement in a Berea core, *Adv. Water Resour.*, *30*, 214–226, doi:10.1016/j.advwatres.2005.05.015.

Qi, R., T. C. LaForce, and M. J. Blunt (2009), Design of carbon dioxide storage in aquifers, *Int. J. Greenh. Gas Control*, *3*(2), 195–205, doi:10.1016/j.ijggc.2008.08.004.

Riaz, A., M. Hesse, H. A. Tchelepi, and F. M. Orr (2006), Onset of convection in a gravitationally unstable diffusive boundary layer in porous media, *J. Fluid Mech.*, *548*, 87–111, doi:10.1017/S0022112005007494.

Roof, J. G. (1970), Snap-off of oil droplets in water-wet pores, *SPE J.*, *10*(1), 85–90.

Suekane, T., T. Nobuso, S. Hirai, and M. Kiyota (2008), Geological storage of carbon dioxide by residual gas and solubility trapping, *Int. J. Greenhouse Gas Control*, *2*(1), 58–64, doi:10.1016/S1750-5836(07)00096-5.

Tschumperlé, D., and R. Deriche (2003), Vector-valued image regularization with PDE's: A common framework for different applications, paper presented at the IEEE Computer Society Conference on Computer Vision and Pattern Recognition, Madison, Wisc.

Xu, T. F., J. A. Apps, and K. Pruess (2003), Reactive geochemical transport simulation to study mineral trapping for CO_2 disposal in deep arenaceous formations, *J. Geophys. Res.*, *108*(B2), 2071, 2071–2084, doi:10.1029/2002JB001979.

M. J. Blunt, A. Paluszny, and C. H. Pentland, Department of Earth Science and Engineering, Imperial College London, London, SW7 2AZ, UK.

S. Iglauer, Department of Petroleum Engineering, Curtin University, Perth, WA 6151, Australia. (stefan.iglauer@curtin.edu.au)